Environmental Science and Ecotechnology 25 (2025) 100566

Contents lists available at ScienceDirect

Environmental Science and Ecotechnology

journal homepage: www.journals.elsevier.com/environmental-science-and-ecotechnology/

Original Research

A pH-responsive production of hydroxyl radical in Fenton process

Pengyi Wang [a, b], Fan Kang [a], Xiangbin Huang [a], Zhipeng Luo [a], Jing Zou [c], Min Yang [d], Meng Sun [e, f], Xin Yu [a, b], Huabin Zeng [a, b, *]

[a] College of the Environment & Ecology, Xiamen University, Xiamen, 361102, China
[b] Fujian Key Laboratory of Coastal Pollution Prevention and Control, Xiamen University, Xiamen, 361102, China
[c] Xiamen Key Laboratory of Municipal and Industrial Solid Waste Utilization and Pollution Control, College of Civil Engineering, Huaqiao University, Xiamen, Fujian, 361021, China
[d] State Key Laboratory of Urban Water Resource and Environment, School of Civil and Environmental Engineering, Harbin Institute of Technology Shenzhen, Shenzhen, 518055, China
[e] Center for Water and Ecology, State Key Joint Laboratory of Environment Simulation and Pollution Control, School of Environment, Tsinghua University, Beijing, 100084, China
[f] State Key Laboratory of Environmental Aquatic Chemistry, Research Center for Eco-Environmental Sciences, Chinese Academy of Sciences, Beijing, 100085, China

ARTICLE INFO

Article history:
Received 10 October 2024
Received in revised form
28 April 2025
Accepted 29 April 2025

Keywords:
pH-responsiveness
Hydroxyl radical
Fenton process
Hydroxylamine
EDTA

ABSTRACT

Efficient management of temporal latency and spatial heterogeneity remains a critical challenge in sensor-based pH regulation for smart water management, primarily due to inherent response delays and mass transfer constraints. In oxidation systems with dynamic pH environments, delayed responses can lead to issues such as cyanide release, unwanted side reactions, or pipe damage. To address these challenges, we propose a "pause-then-adjust" control strategy, exploiting the pH-responsive generation of hydroxyl radicals (•OH) in a modified Fenton reaction system. This system utilizes hydroxylamine as an electron donor and ethylenediaminetetraacetic acid (EDTA) as a stabilizer for iron ions. Within the pH range of 7.0–10.0, the coexistence of $[Fe^{2+}\text{-EDTA}]^{2-}$ and $[Fe^{3+}\text{-OH-EDTA}]^{2-}$ complexes facilitates efficient electron transfer, resulting in the selective and sustained production of •OH radicals. The inherent pH-responsiveness of this strategy enables rapid and spatially coherent adjustments, offering a robust supplementary method for addressing complex and evolving requirements in advanced water treatment systems.

1. Introduction

Smart water management has recently attracted increasing attention due to its potential to revolutionize the traditional water industry by elevating its informatization level [1]. This new approach aims to streamline business operations, enable scientific management practices, and improve service quality in water management. In applying smart water management to water treatment plants, a crucial aspect involves rendering the process 'intelligent' and finely controlling it through digital regulation. The primary strategy currently involves gathering water quality parameters through various sensors and responding according to a pre-established feedback mechanism [2]. However, latency is inevitable in the entire 'reflex arc'—from the monitoring unit and computing center to the response unit. Furthermore, concerning the response involving dosing chemical reagents, the spatial unevenness induced by mass transfer may lead to unsatisfactory treatment efficiency in the microenvironment. Although these problems can be alleviated by resetting the feedback logic or enhancing mechanical agitation, such efforts may increase chemical dosages or energy consumption. Thus, a desirable alternative is to explore regulatory strategies that ensure immediate responsiveness and spatial synchronization when the monitored parameter deviates from the preset value.

As an efficient process for generating •OH, the Fenton process has played pivotal roles in various domains, such as water purification [3], molecular synthesis [4], and tumor therapy [5]. However, due to inherent properties and, in some cases, the production of

* Corresponding author. College of the Environment & Ecology, Xiamen University, Xiamen, 361102, China.
E-mail address: HuabinZeng@xmu.edu.cn (H. Zeng).

https://doi.org/10.1016/j.ese.2025.100566

carboxylic acids during the degradation process of organics, the solution pH typically deviates from the initial pH as the reaction progresses [6]. Scientists and engineers have sought various Fenton systems with wider pH ranges for decades to avoid additional pH regulation before treating targeted water [7]. Although these processes have functioned well in most cases, there have also been a few instances in which such pH deviations have serious consequences. For example, system acidification in cyanide-containing wastewater may pose a potential risk of cyanide leakage [8]. Moreover, when employing the Fenton reaction for the pH-dependent synthesis process of specific chemicals, the deviation of the solution pH might induce the unwanted formation of side products [9]. Additionally, abrupt pH changes within the water distribution system would cause significant damage to cast iron pipes, ultimately shortening their longevity [10]. Therefore, pH-responsive generation of $^{\bullet}OH$ at a specific pH level would be advantageous in the Fenton process, enabling the immediate termination of the $^{\bullet}OH$ utilization reaction once the solution pH deviated from the preset value. Thus, a 'smart Fenton system' could feature a pause-then-adjust approach to address the latency between monitoring and response, as well as the spatial non-uniformity induced by insufficient stirring, to ensure stable operation within the designated pH parameters.

To establish such a system with target characteristics, we considered two interesting types of enhanced Fenton processes: reductant-enhanced Fenton and organic-chelated Fenton. In the reductant-enhanced Fenton system, hydroxylamine (HA) as the reducing agent enhances the reduction process of Fe^{3+}, accompanied by the Fe^{2+} regeneration for continuous H_2O_2 activation in the Fenton process [11]. In the organic-chelated Fenton system, the complexing agent can broaden the soluble pH range of iron ions, thus avoiding sedimentation of iron-containing sludge [12,13]. Based on the Nernst equation, the H_2O_2 activation by Fe^{2+} (oxidation process) is acid-favorable, while the Fe^{3+} reduction process (reduction process) favors alkaline conditions. In theory, the Fenton process enhanced by the synchronous addition of HA and a chelating agent is simultaneously influenced by both processes and may have a narrow applicable pH range because of the different pH adaptability between these two determining steps.

Herein, we construct an enhanced Fenton process using HA as the reducing agent, employing ethylenediaminetetraacetic acid (EDTA) to tune the redox property of the Fe^{3+}/Fe^{2+} redox pair. We clarify the contribution of $^{\bullet}OH$ using electron spin resonance (ESR) analysis and quenching experiments. We also reveal the effect of solution pH on the $^{\bullet}OH$ generation in the system using benzoic acid (BA) as $^{\bullet}OH$ probe, and the pH-responsive property of the system is further investigated using density functional theory (DFT) analysis. We conclude with an in-depth discussion of the application potential of the technology in smart water management.

2. Experimental section

2.1. Chemicals

A complete list of reagents is provided in Supplementary Material Text S1.

2.2. Setup and experiment

All the solutions used in this study were prepared with Milli-Q water. Batch experiments were conducted in 200 mL beakers at room temperature and atmospheric pressure. EDTA, $FeSO_4$, HA, and BA were first added to the system during the experiment. After adjusting to a predetermined pH value, oxidizer H_2O_2 was added, and the timing began. The pH was continuously monitored with a pH meter throughout the experiment and performed to the index value at any time using NaOH or H_2SO_4. After a predetermined time interval, a 2 mL sample was removed into the centrifuge tube with a pipette, immediately quenched with excess ethanol aqueous solution, and filtered by 0.22 μm membrane before analysis.

2.3. Detection of BA

The BA probe substance was measured by high-performance liquid chromatography (HPLC, LC-20AD, Shimadzu) coupled with a photodiode array detector. The mobile phase used a ratio of 47:53 1‰ acetic acid and chromatograph-grade methanol at a constant flow rate of 0.8 mL min^{-1}, the temperature of the chromatographic column was 35 °C, and the detection wavelengths were set at $\lambda = 228$ nm.

2.4. Electron spin resonance spectroscopy analysis

ESR was used to identify the primary reactive oxygen species (ROS) $^{\bullet}OH$. Before the decay of the $^{\bullet}OH$ in the system, 5,5-dimethyl-1-pyrroline N-oxide (DMPO) was added as the trapping agent, forming adducts with the $^{\bullet}OH$ to be measured.

2.5. Determination of other components of the system

The concentration of Fe^{2+} was determined using the 1,10-phenanthroline method, and the absorbance was measured at 510 nm after 10 min of color development [14]. For Fe^{3+}, the maximum absorption peak at 300 nm was used to determine its concentration (Supplementary Material Text S2). The concentration of H_2O_2 was determined using the titanium oxide sulfate method, and the absorbance was measured at 400 nm after adding the color developer for 10 min [15]. HA was reacted with acetone to form acetone oxime, and the concentration of acetone oxime was determined by HPLC [16] (mobile phase: methyl alcohol:0.2‰ formic acid = 30%:70%; measure wavelength 220 nm; sample volume 20 μL; flow rate 0.2 mL min^{-1}). The EDTA concentration was determined by high performance liquid chromatography—mass spectrometry (HPLC—MS) experiments.

2.6. Statistical analysis

All degradation data were obtained through two parallel experiments. The degradation of BA was quantified by calculating the ratio of the BA concentration at time 't' (C_t) to the initial BA concentration (C_0). We employed the arithmetic mean of the results from the two parallel experiments, and the standard deviation (calculated by the STDEVA function) was used to generate error bars. MINTEQ 3.1 was used to simulate the species of the [Fe-EDTA] complexes across various pH ranges.

2.7. DFT analysis

The DFT calculations were performed using the Gaussian 16 (A.03) software package [17]. Considering the involvement of transition metals in the computational process, we adopted a robust PBE1PBE functional combined with a mixed basis set [18,19]. The Fe atoms were treated with the Stuttgart-Dresden (SDD) pseudopotential basis set, while the remaining elements were optimized using the 6-311G (d,p) basis set. This allowed us to obtain stable wave functions and structures for the target ligands. The calculations were conducted with the solvation model of density (SMD) to account for the solvent effects of water on the reactions [20]. The obtained wave functions were further analyzed using Multiwfn 3.8 (dev) software to obtain information such as local

electron attachment energy (LEAE) [21,22], average local ionization energy (ALIE) [23,24], highest occupied molecular orbital (HOMO), lowest unoccupied molecular orbital (LUMO), charge distributions [25], and intermolecular weak interactions [26]. The isosurface plots of various real-space functions were rendered using visual molecular dynamics (VMD) software based on cube files exported from Multiwfn [27,28].

3. Results & discussion

3.1. BA degradation in Fe^{2+}/EDTA/HA/H_2O_2 system

We investigated the degradation of BA (40 μM) in the Fe^{2+}/EDTA/HA/H_2O_2 system at pH 9.0; that is, in addition to HA (0.5 mM), Fe^{2+} (20 μM), EDTA (20 μM), and H_2O_2 (1.0 mM), the reaction system was manually controlled at pH 9.0 ± 0.2 (Supplementary Material Text S3). 69% of BA was rapidly degraded in 60 min, with a first-order kinetic constant of 0.072 min^{-1} (k_1) (Fig. 1a). Interestingly, BA degradation did not occur in the other systems, indicating the necessity of each component in producing ROS.

ESR technology using DMPO as a trapping agent was further employed to identify ROS in the system [29]. Similar to the results of degradation experiments, only in the Fe^{2+}/EDTA/HA/H_2O_2 system were four classical peaks detected at a ratio of 1:2:2:1 (Fig. 1b), which was considered to be a sign of the •OH presence [30]. Using methanol (MeOH, for inhibiting •OH), tert-butyl alcohol (TBA, for inhibiting •OH), and chloroform (for inhibiting $•O_2^-$) as scavengers [13], the quenching experiment revealed the dominant contribution of •OH in BA degradation. It should be pointed out that $•O_2^-$ may play a negligible role in the process, owing to its weak inhibition of BA degradation by adding 10 mM chloroform and hardly any peak in the ESR data (Supplementary Material Fig. S2). Both MeOH and TBA impeded BA degradation; the k_1-values of BA degradation decreased from 0.072 to 0.015 and 0.015 min^{-1} (Supplementary Material Fig. S1; Fig. 1c). High-valance iron is also one of the active oxidation species commonly seen in such systems [31,32], but no methyl phenyl sulfone ($PMSO_2$) was generated in the methyl phenyl sulfoxide (PMSO) probe experiment (Supplementary Material Fig. S3), which proved that there was no high-valance iron formation in the system.

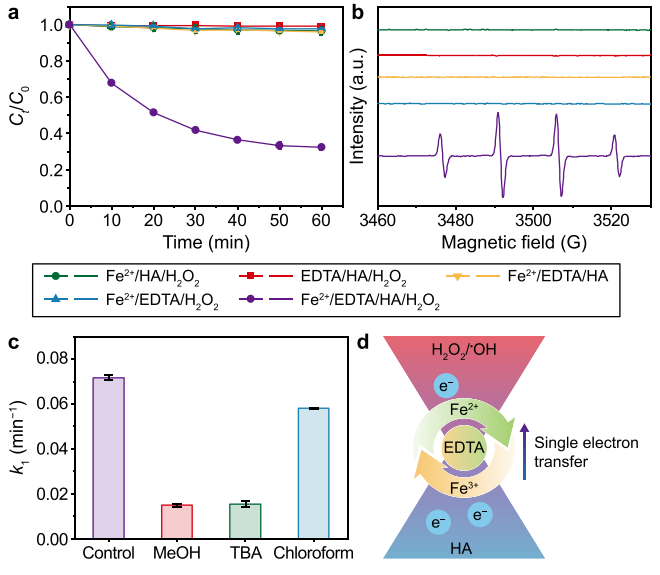

Fig. 1. **a**, Benzoic acid (BA) degradation in various systems. **b**, Electron spin resonance (ESR) signals for •OH in various systems [with 100 μM 5,5-dimethyl-1-pyrroline N-oxide (DMPO)]. **c**, k_1-value for BA degradation under quenching conditions. **d**, Schematic of Fe^{2+}/EDTA/HA/H_2O_2 system. Experimental condition: [BA] = 40 μM; [Fe^{2+}] = 20 μM; [ethylenediaminetetraacetic acid (EDTA)] = 20 μM; [hydroxylamine (HA)] = 0.5 mM; [H_2O_2] = 1.0 mM; [Chloroform] = [Methanol (MeOH)] = [tert-butanol (TBA)] = 10 mM; Solution pH = 9.0 ± 0.2.

In summary, •OH was produced to degrade the probe (BA) in the Fe^{2+}/EDTA/HA/H_2O_2 system at pH 9.0. In the system, about 69% of 40 μM BA was degraded (27 μM), which was higher than the Fe^{2+} dosage (20 μM). It is plausible that one-unit Fe^{2+} activated H_2O_2 produced one-unit •OH to degrade one-unit BA, indicating the occurrence of iron cycling in the reaction process. In the presence of EDTA, Fe^{2+}/Fe^{3+} ions can exist in an alkaline solution, facilitating the transfer of a single electron from HA to H_2O_2. This enables the continuous production of •OH, allowing the continuous production of the •OH (Fig. 1d) [10,33]. In the process, each constituent plays a distinct role, with H_2O_2 serving as •OH precursor, Fe^{3+}/Fe^{2+} redox pair acting as a catalyst, EDTA functioning as a catalyst stabilizer, and HA serving as an electron reservoir.

3.2. pH-responsive production of •OH

The Fenton reaction is recognized for its pH-dependent characteristics, wherein the ROS generation occurred exclusively within a specific pH range, typically within pH 2.0–4.0 for the traditional Fenton system [11,34]. Therefore, we investigated BA degradation in the Fe^{2+}/EDTA/HA/H_2O_2 system at different pH levels. The Fe^{2+}/EDTA/HA/H_2O_2 system demonstrated minimal degradation of BA under acidic conditions, with the degradation ratio below 1% (k_1 < 0.001) within the pH range of 3.0–5.0 during a 60-min timeframe (Fig. 2a). With the increase in pH, the degradation ratio of the system also gradually increased (10% for pH 6.0 and 43% for pH 7.0); correspondingly, the k_1-value increased from 0.002 to 0.009 (Fig. 2c). Until the pH increased to 8.0–9.0, the BA degradation effect of the system reached the best; nearly 70% of BA in the system was degraded within 60 min with the k_1-value of 0.021 and 0.029 (Fig. 2a). However, a further increase in the pH resulted in a downward trend in the degradation ratio of BA. When the pH increased to 10.0, the degradation rate of BA in 60 min decreased by 32% (k_1 = 0.012) and further increasing to 11 resulted in a 53% decrease (k_1 = 0.002). At pH 12, BA in the system was hardly degraded (Fig. 2b). The performance of the system on BA degradation indicated an interestingly undocumented phenomenon—namely, the novel Fenton system occurred at a narrow applicable pH range (7.0–10.0) for •OH production. In addition, the ESR results revealed a similar tendency in the •OH occurrence as a function of solution pH (Supplementary Material Fig. S4).

This phenomenon could be explained by existing forms of variation of [Fe^{3+}-EDTA] or [Fe^{2+}-EDTA] complexes at different pH values, which was simulated by MINTEQ 3.1 software (Supplementary Material Fig. S5) [35,36]. As the solution pH increased from 7.0 to 10.0, the existing form of [Fe^{2+}-EDTA] complexes shifted from the form of [Fe^{2+}-EDTA]$^{2-}$ to [Fe^{2+}-OH-EDTA]$^{3-}$, and the [Fe^{3+}-EDTA] complexes tended to exist in the form of [Fe^{3+}-OH-EDTA]$^{2-}$ rather than [Fe^{3+}-EDTA]$^{-}$. To better analyze the inherent relationship of the [Fe-EDTA] complexes existing form with BA degradation, the existing percentages of [Fe^{2+}-EDTA]$^{2-}$ and [Fe^{3+}-OH-EDTA]$^{2-}$ were plotted as a function of solution pH (Fig. 2c). Comparing the curve of k_1-value with the product of P [(Fe^{2+}-EDTA)$^{2-}$] and P [(Fe^{3+}-OH-EDTA)$^{2-}$] revealed that variations of the kinetic constants as a function of solution pH were highly consistent with the trends of P [(Fe^{2+}-EDTA)$^{2-}$] × P [(Fe^{3+}-OH-EDTA)$^{2-}$] as a function of pH. The linear fitting results depicted in Fig. 2d revealed a robust linear correlation, with high confidence (R^2 = 0.9598), between the product and k_1 across pH levels of 3.0–12.0.

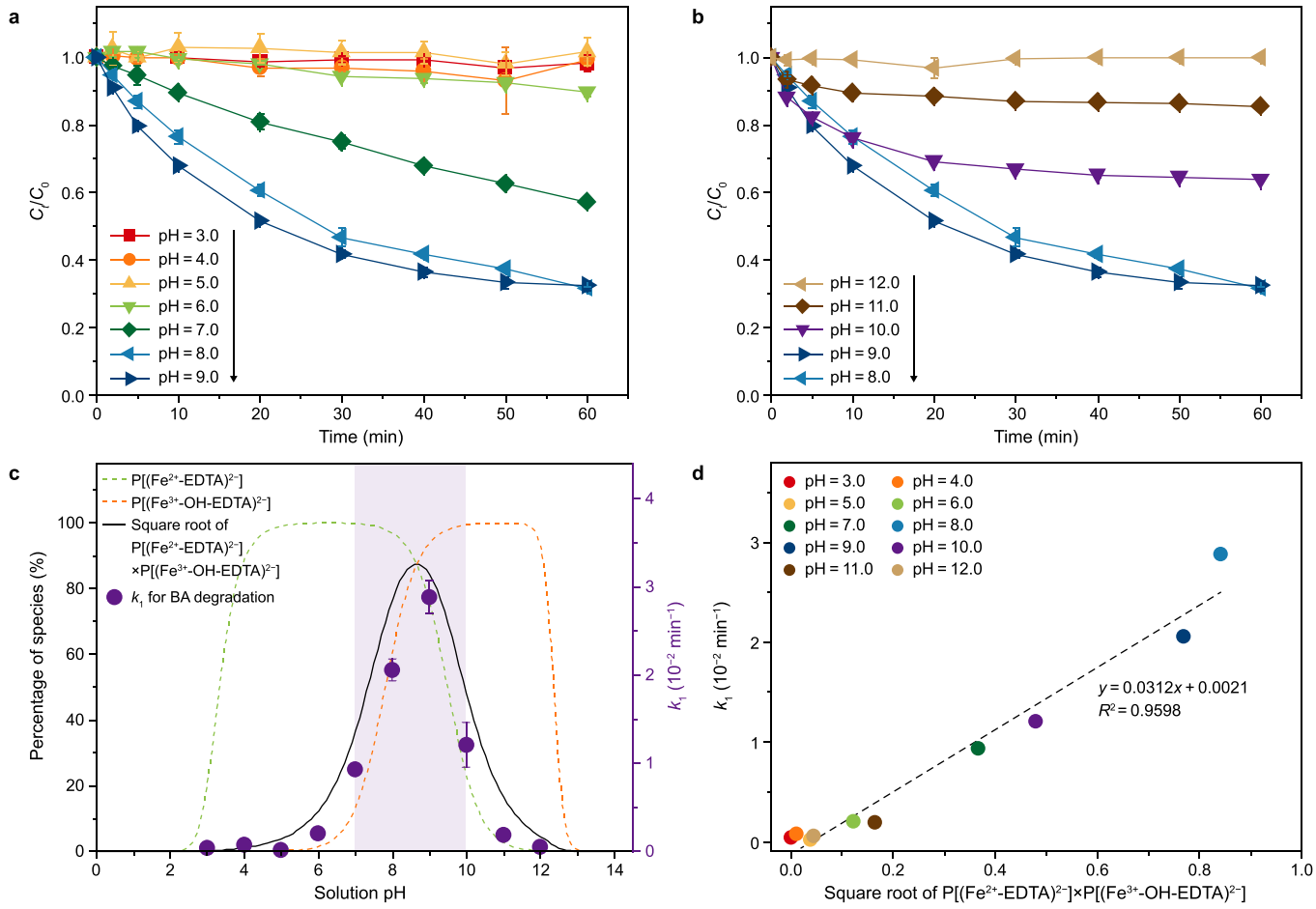

Fig. 2. **a**–**b**, Effect of pH on the degradation ratio of BA: pH from 3.0 to 9.0 (**a**) and pH from 8.0 to 12.0 (**b**), the arrow direction indicates the increased degradation ratio of BA. **c**, Proportion of $[Fe^{2+}\text{-EDTA}]^{2-}$ for all $[Fe^{2+}\text{-EDTA}]$ complexes, proportion of $[Fe^{3+}\text{-OH-EDTA}]^{2-}$ for all $[Fe^{3+}\text{-EDTA}]$ complexes, their product, and the first-order kinetic constant (k_1). The shadow is the applicable pH range for the Fe^{2+}/EDTA/HA/H_2O_2 system. **d**, Linear fitting of the product of complexes fraction and the k_1 of BA. Experimental condition for panels **a** and **b**: [HA] = 1 mM; $[Fe^{2+}]$ = 20 μM; [EDTA] = 20 μM; [BA] = 40 μM; $[H_2O_2]$ = 1 mM; Solution pH = 3.0–12.0.

The modulation of the BA degradation rate was principally regulated by two determining steps: the activation of H_2O_2 through Fe^{2+} and the reduction of Fe^{3+} by HA. These two steps were consistent with the second-order kinetic model [37], and a sequence of derivations reported in Text S4 (Supplementary Material) deduced that the k_1 of BA degradation in the Fe^{2+}/EDTA/HA/H_2O_2 system exhibited a linear correlation with the square root of the product resulting from the proportion of reaction-suitable complexes. The product of P $[(Fe^{2+}\text{-EDTA})^{2-}]$ and P $[(Fe^{3+}\text{-OH-EDTA})^{2-}]$ had a strong consistency with k_1 (Fig. 2c and d) [38]. Hence, establishing that $[Fe^{2+}\text{-EDTA}]^{2-}$ had the highest reactivity with H_2O_2 and that $[Fe^{3+}\text{-OH-EDTA}]^{2-}$ was the most reducible by HA could explain the particularly suitable pH range of this system (these two points are discussed in detail in the next section). On the one hand, in an excessively acidic environment (pH < 7.0), the $[Fe^{3+}\text{-EDTA}]$ complexes failed to adopt the form of $[Fe^{3+}\text{-OH-EDTA}]^{2-}$, which was the most favorable for HA reduction, resulting in inefficient circulation of the [Fe-EDTA] complexes. On the other hand, in an overly alkaline environment (pH > 10.0), the $[Fe^{2+}\text{-EDTA}]$ complexes were unable to adopt the form of $[Fe^{2+}\text{-EDTA}]^{2-}$, which was the most conducive to the activation of H_2O_2, resulting in difficult to generate •OH and the degradation of BA.

3.3. Reactivity analysis of [Fe-EDTA] complexes

The results presented above suggest that the special narrow pH-suitable levels of the Fe^{2+}/EDTA/HA/H_2O_2 system were due to the existence of different forms of [Fe-EDTA] complexes under different pH conditions. Thus, DFT calculations determined the morphologic active sites and their reactivity. Here, we focused on the $[Fe^{2+}\text{-EDTA}]^{2-}$ and $[Fe^{2+}\text{-OH-EDTA}]^{3-}$ species within $[Fe^{2+}\text{-EDTA}]$ complexes, as well as the $[Fe^{3+}\text{-EDTA}]^{-}$ and $[Fe^{3+}\text{-OH-EDTA}]^{2-}$ species within $[Fe^{3+}\text{-EDTA}]$ complexes. Analysis of the electron spin density (Supplementary Material Fig. S6) revealed that the single electrons of all complexes were mainly distributed on the central iron atom and the four oxygen atoms around it, with the main distribution locations of single electrons being the active sites of the molecule. Following frontier orbital theory (Supplementary Material Fig. S7), atoms with larger electron clouds occupied the HOMO energy level or LUMO energy level, which were more likely to become electrophilic (nucleophilic) reaction sites. The atomic local ionization energy (ALIE) of the $[Fe^{2+}\text{-EDTA}]$ complexes showed that the regions with weak electron-binding ability and those that could easily become electron-loss reaction sites in the molecule were mainly distributed on the four oxygens of EDTA and the oxygens connected with hydroxyl groups (Fig. 3a). The local

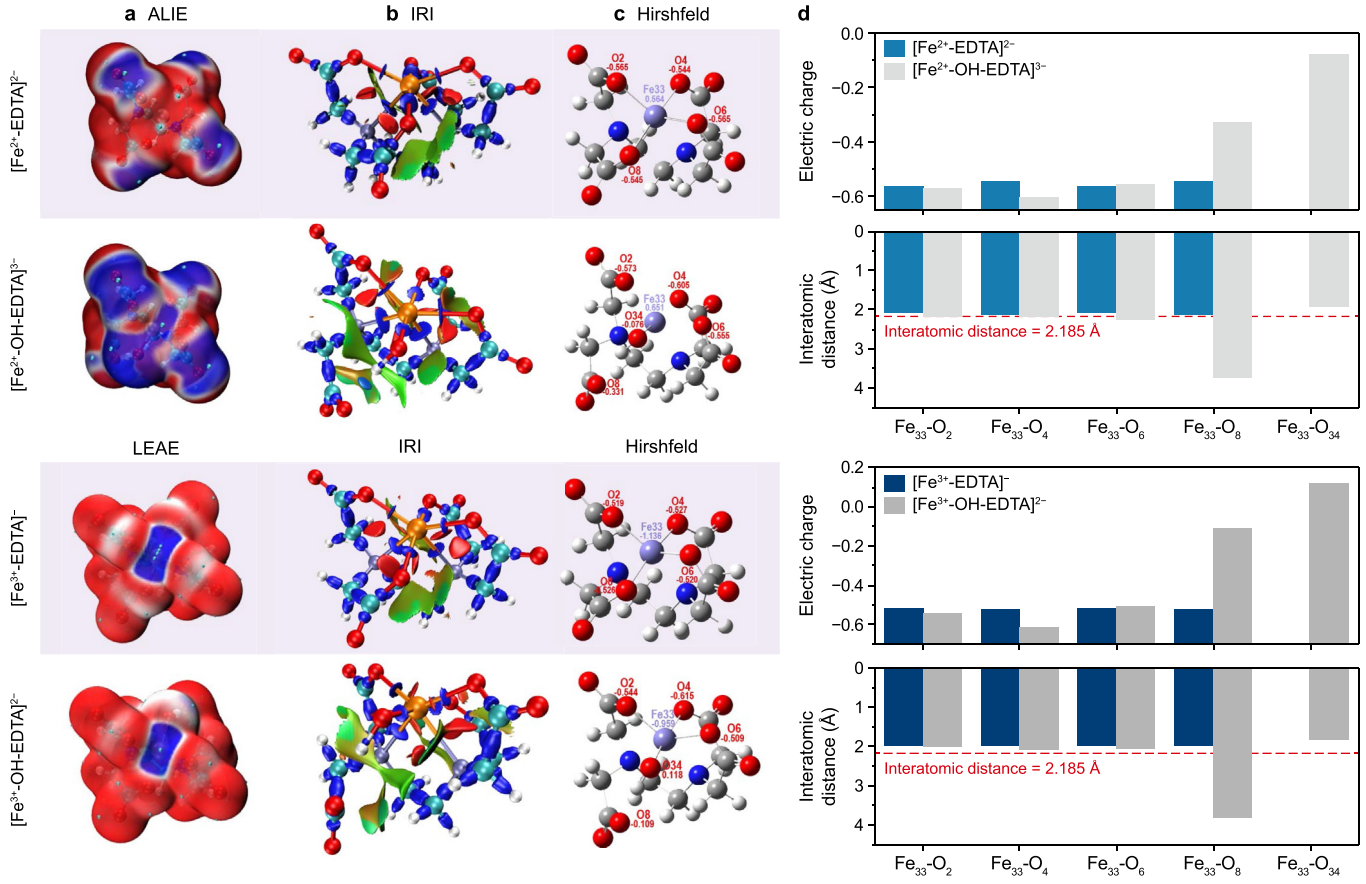

Fig. 3. Theoretical calculation analysis of [Fe-EDTA] complexes by density functional theory (DFT) analysis. **a**, Average local ionization energy (ALIE) or local electron attachment energy (LEAE) analysis of frontier orbit theory; **b**, Interaction region indicator (IRI) analysis of the weak interatomic force; **c**, Atomic charge and interval analysis based on Hirshfeld; **d**, Histogram based on atomic charge and spacing. When the molecular distance was below 2.185 Å, the ferro-oxygen bond can be considered.

electron attachment energy (LEAE) of the [Fe^{3+}-EDTA] complexes showed that there was a high-energy unoccupied orbital at the central iron atom, which has stronger electrophilicity, tends to be attacked by nucleophile, and becomes the reaction site for electron acquisition. However, HOMO (LUMO) ALIE or LEAE analyses did not consider interatomic interactions and steric hindrances. Therefore, we included an interatomic weak force analysis (interaction region indicator, IRI) (Fig. 3b), which demonstrated that the interatomic repulsive forces gradually increased from the blue to red regions, resulting in steric hindrance that hindered electron transport (Supplementary Material Fig. S8). By accounting for steric hindrance, we obtained a more accurate ferro-oxygen distance and atomic charge distribution (Fig. 3c), which can be used to compare the reactivity of the [Fe-EDTA] complexes.

For the [Fe^{2+}-EDTA] complexes, ALIE analysis showed that the electron-donating reaction sites were mainly distributed on the four oxygen atoms adjacent to the central iron atom. When the steric hindrance was neglected, there were more possible electron donor reaction sites on the surface of the [Fe^{2+}-OH-EDTA]$^{3-}$ states (Fig. 3a). However, there was some weak force between atoms (Fig. 3b), and the introduction of -OH reduced the positive charge of the iron atoms (Fig. 3c). The introduction of -OH led to a decrease in the positive charge density of the iron atoms (Fig. 3d), accompanied by an increase in the distance between the iron atoms and the surrounding oxygen atoms [39]. Fe-O bonds became infeasible when this distance exceeded the bonding distance between iron and oxygen. The electron transport efficiency among bonded atoms exhibited a substantially higher value than that observed among unbonded atoms. Compared with [Fe^{2+}-EDTA]$^{2-}$, although Fe_{33} in the center of [Fe^{2+}-OH-EDTA]$^{3-}$ formed a new bond with O_{34}, O_{34} itself carried a minimal negative charge, exhibiting little repulsive force on electrons and weak electron-donating ability. Consequently, it was difficult for O_{34} to serve as the electron-donating reaction site required for the reaction with H_2O_2. However, the increased distance of Fe_{33} with the original oxygen atoms O_2, O_4, O_6, and O_8 hindered the formation of Fe-O bonds, losing the better potential reaction sites that carried more negative charges. Therefore, the reaction ability of [Fe^{2+}-EDTA]$^{2-}$ with H_2O_2 was stronger than that of [Fe^{2+}-OH-EDTA]$^{3-}$.

For the [Fe^{3+}-EDTA] complexes, the reaction site of the electron was also distributed on the central iron atom and the four adjacent oxygen atoms. The possible electron reaction sites were distributed around Fe_{33} with or without introducing -OH. However, the iron atom was located in the center of the molecule; it was difficult to directly contact the electron donor HA and obtain electrons, which required electron transfer by the oxygen atoms (Fig. 3a). Based on our analysis of the weak interatomic force (Fig. 3b), the introduction of -OH would only increase the distance between O_8 and Fe_{33} to the point that bonding cannot be achieved, whereas the spacing and charge capacity of the remaining O_2, O_4 and O_6 would not increase significantly. Compared with O_8, the newly introduced O_{34} has a closer distance with Fe_{33}, which was more conducive to the formation of ferro-oxygen bonds (Fig. 3d), and its charge was positive (Fig. 3c), which can attract electrons and is more suitable as

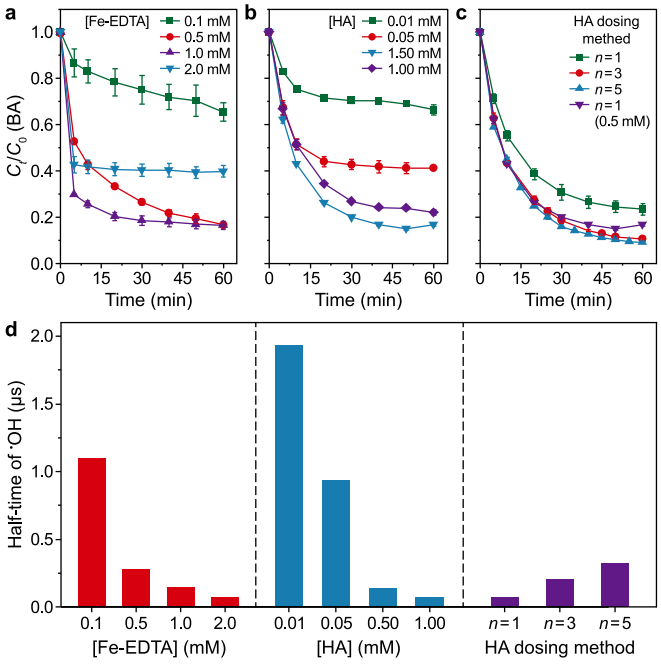

Fig. 4. BA degradation ratio in various systems. **a**, High [Fe^{2+}-EDTA] complexes concentration (without HA); **b**, Different HA concentration; **c,** Different HA addition modes; **d,** •OH half-life in different systems. Experimental condition for panels **a**: [BA] = 40 μM; [H_2O_2] = 1 mM; [Fe^{2+}] and [EDTA] = 0.1–2.0 Mm; pH = 9.0 ± 0.2; **b**: [BA] = 40 μM; [H_2O_2] = 1 mM; [Fe^{2+}] = 20 μM; [EDTA] = 20 μM; [HA] = 0.01–1.00 mM; pH = 9.0 ± 0.2; **c**: [BA] = 40 μM; [H_2O_2] = 1 mM; [Fe^{2+}] = 20 μM; [EDTA] = 20 μM; [HA] = 1.00/0.50 mM; pH = 9.0 ± 0.2.

a reaction site for obtaining electrons. Therefore, compared with [Fe^{3+}-EDTA]$^-$, [Fe^{3+}-OH-EDTA]$^{2-}$ has a stronger reaction capacity with HA.

3.4. Parameter optimization

For the Fe^{2+}/EDTA/H_2O_2 system, low concentration (20 μM) of [Fe^{2+}-EDTA] could not promote the generation of •OH (Fig. 1a). We attributed this outcome to the inefficient circulation of [Fe^{2+}-EDTA]/[Fe^{3+}-EDTA] complexes. However, previous work has shown that a high concentration of [Fe^{2+}-EDTA] complexes (1 mM) could also induce the formation of •OH [13]. Therefore, we investigated the effect of a high concentration of [Fe^{2+}-EDTA] complexes on the degradation ratio of BA (Fig. 4a). Within a certain concentration range (0.1–1.0 mM), increasing the concentration of [Fe^{2+}-EDTA] complexes enhanced the degradation ratio. However, the [Fe^{2+}-EDTA] complexes itself was also an organic matter in the degradability range of •OH, given its high reaction rate with •OH ($k = 5 \times 10^9$ M^{-1} S^{-1}) [40]. In an environment with high complex content, the presence of [Fe^{2+}-EDTA] complexes would consume the generated •OH and reduce the chance of contacting the target substance, BA, degrading it. This would result in a competitive effect between [Fe^{2+}-EDTA] complexes and BA for •OH. Under experimental conditions, when the [Fe^{2+}-EDTA] complexes concentration reached 2 mM, the degradation ratio of BA decreased to 58% in the first 10 min, with no BA degradation. Thus, although a high concentration of complex agents could facilitate the production of •OH, it would concurrently result in diminished utilization efficiency.

Similarly, the concentration of HA in the system also affected the degradation effect. For the low concentration of [Fe^{2+}-EDTA] complexes, a stepwise increase in the HA dosage of the system gradually increased the BA removal ratio. As the concentration of HA increased, the degradation ratio of BA also exhibited a pattern of initially increasing before decreasing (Fig. 4b). HA mainly existed in the form of NH_2OH at pH 9.0, and NH_2OH and •OH also had high reaction rate constants ($k = 9.5 \times 10^9$ M^{-1} S^{-1}) [41]. Hence, beyond a certain threshold, with the increase of HA, the ability to compete •OH would also strengthen, leading to a reduction in the degradation ratio of BA [11,42]. However, HA was an essential reducing agent in the system, so the mode of HA changed from single-dosing to multiple-dosing addition during the reaction; that is, the required HA was divided into several equal parts and added gradually during the reaction [37]. When the total amount of HA was fixed at 1 mM, $n = 3$ and $n = 5$ achieved a removal ratio of 89% and 90%, which was about 14% higher than that at $n = 1$ (77%) and about 7% higher than with 0.5 mM HA at $n = 1$ (83%) (Fig. 4c).

The half-life of the •OH can illustrate its survival time from formation to annihilation in the system, and the longer its survival time, the more likely it was to degrade the targeted pollutant. The •OH half-life was estimated based on the reaction rate constants of different substances with •OH, as illustrated in Text S5 (Supplementary Material). An increase in the initial concentrations of [Fe^{2+}-EDTA] complexes and HA shortened the half-life of •OH (Fig. 4d), thus reducing the utilization efficiency of •OH. However, the lack of a reducing agent would have caused the early termination of •OH generation because of poor iron circulation; thus, we employed the fractional dosing mode to add HA. When the HA was split into five parts and added at the same time intervals, the half-life of •OH was significantly increased to 0.32 μs, which was about four times that of the single-dosing mode.

In summary, combining the degradation effects of different dosages (Supplementary Material Fig. S9) and the calculation of •OH half-life (Fig. 4d), we optimized the optimal dosages of each component of the system as follows: $H_2O_2 = 1$ mM; $Fe^{2+} = 20$ μM; EDTA = 20 μM; HA = 1 mM ($n = 5$).

3.5. System composition analysis

HA in the Fe^{2+}/EDTA/HA/H_2O_2 system fate to be degraded into small molecule inorganic substances, which were harmless and convenient for subsequent treatment, and N_2 had the highest proportion in 30 min (83%), and a few converted to NO_2^-, NO_3^-, and N_2O (Supplementary Material Fig. S10) [16]. The iron ion stabilizer EDTA, an organic matter, could be degraded by •OH during the reaction process. The primary intermediates formed during this degradation were ethylenediamine triacetate iron complex (Fe-ED3A), ethylenediamine diacetate iron complex (Fe-EDDA), and iminodiacetic acid (IMDA). Ultimately, it is thoroughly mineralized into innocuous inorganic molecules, such as CO_2 and H_2O (Supplementary Material Fig. S11) [43,44]. The influence of ventilation conditions was discussed in Supplementary Material Text S6 (Supplementary Material Fig. S12), and the difference between the degradation ratio in 60 min of nitrogen injection, oxygen injection, and air injection could be ignored. We tried other complexing agents, ethylenediamine-N,N′-disuccinic acid (EDDS), nitrilotriacetic acid (NTA), and sodium citrate, but did not observe experimental outcomes similar of EDTA (Supplementary Material Fig. S13).

3.6. Support for smart water management

In the Fenton system, the generation of •OH was the oxidation process, whereas the cycling of trivalent iron was the reduction process. The discrepancy in their suitable pH ranges explains the narrow optimal pH range of the Fe^{2+}/EDTA/HA/H_2O_2 system. Unlike the existing enhanced Fenton system, which prioritizes broadening

the pH range, the unique advantage of the Fe^{2+}/EDTA/HA/H_2O_2 system is its sensitivity to changes in pH [45]. This optimized system could be applied to special pH-dependent scenarios in smart water management, such as cyanide-containing wastewater. The system is continuously acidified by a process of advanced oxidation, which would cause the cyanide to escape as gas, causing significant risks to human health [46–49]. However, in Fe^{2+}/EDTA/HA/H_2O_2 system, the generation of $^{\bullet}OH$ would pause at about pH = 7.0 due to exceeding the appropriate pH range, recovering when the pH is adjusted back (Supplementary Material Fig. S14). This self-protection mechanism can effectively avoid further acidification of the system and keep the system in a moderately alkaline pH range to ensure the safety of the cyanide removal process [50]. In our experiments, when potassium ferricyanide was used as the interference, the degradation ratio of BA in the system was still maintained in a relatively stable range (Supplementary Material Fig. S15), and similar results were obtained in experiments with actual wastewater (mainly containing copper cyanide complex, Na^+, and Zn^{2+}) (Supplementary Material Fig. S16).

Therefore, the optimized Fenton system has the potential as an outstanding counterplan for smart water management to combat similar issues with wastewater, which has been facing a firm demand for immediate responsiveness and spatial synchronization of its pH. Furthermore, acidic wastewater poses a significant threat of accelerated corrosion to piping systems, which may lead to a considerable reduction in the service life of the equipment. Conversely, the Fe^{2+}/EDTA/HA/H_2O_2 system effectively stabilized the pH value of the wastewater treatment process within neutral or alkalescency, thus avoiding the system acidification problems usually associated with advanced oxidation and less burden on the equipment than traditional Fenton.

4. Conclusion

In this work, the Fe^{2+}/EDTA/HA/H_2O_2 system was constructed to address pH-dependent scenarios in smart water management. Within the system, only the H_2O_2 activation by Fe^{2+} and Fe^{3+} reduction by HA simultaneously occurred, and $^{\bullet}OH$ could be continuously generated. The addition of 20 μM Fe^{2+} resulted in 69% of 40 μM of BA becoming degraded at pH 9.0, confirming iron circulation in the system. Density function theory revealed that the species of the [Fe-EDTA] complexes affected its reactivity. This was caused by bond length, charge amount, steric hindrance, and other factors. Due to their stronger electron-transferring capacity, [Fe^{2+}-EDTA]$^{2-}$ species had a higher activity of turning H_2O_2 into $^{\bullet}OH$, while [Fe^{3+}-OH-EDTA]$^{2-}$ species was more smoothly reduced by HA. This difference in pH required for the existence of these two forms allowed for the pH-responsiveness of the system, utilizing a "pause-then-adjust" strategy to cope with changes in pH. In summary, the Fe^{2+}/EDTA/HA/H_2O_2 system could address the latency between monitoring and response and the spatial non-uniformity induced by insufficient stirring to ensure stable operation within the designated pH parameters. The pH responsiveness made the system an immediately responsive and spatially synchronized supplementary method that could be used to address increasingly sophisticated water treatment requirements.

CRediT authorship contribution statement

Pengyi Wang: Writing - Review & Editing, Writing - Original Draft, Methodology, Investigation. **Fan Kang:** Writing - Original Draft, Investigation, Data Curation. **Xiangbin Huang:** Writing - Review & Editing, Investigation. **Zhipeng Luo:** Visualization, Investigation. **Jing Zou:** Validation, Supervision. **Min Yang:** Validation, Supervision. **Meng Sun:** Validation, Supervision. **Xin Yu:** Supervision, Resources, Funding Acquisition. **Huabin Zeng:** Resources, Project Administration, Funding Acquisition, Conceptualization.

Declaration of competing interest

The authors declare that they have no known competing financial interests or personal relationships that could have appeared to influence the work reported in this paper.

Acknowledgments

The authors would like to thank Professor Ranwen Ou and Yinzhou Luo for their invaluable assistance during the revision process. This work was supported by the National Natural Science Foundation of China (No. 52400097), the Open Project of State Key Laboratory of Urban Water Resource and Environment from Harbin Institute of Technology (No. QA202446), and the Nanqiang Young Talents Supporting Program from Xiamen University.

Appendix A. Supplementary data

Supplementary data to this article can be found online at https://doi.org/10.1016/j.ese.2025.100566.

References

[1] M. Singh, S. Ahmed, IoT based smart water management systems: a systematic review, Mater. Today Proc. 46 (2021) 5211–5218.
[2] S.W. Lee, S. Sarp, D.J. Jeon, J.H. Kim, Smart water grid: the future water management platform, Desalin. Water Treat. 55 (2) (2014) 339–346.
[3] X.J. Yang, X.M. Xu, J. Xu, Y.F. Han, Iron oxychloride (FeOCl): an efficient Fenton-like catalyst for producing hydroxyl radicals in degradation of organic contaminants, J. Am. Chem. Soc. 135 (43) (2013) 16058–16061.
[4] M.S. Chen, M.C. White, A predictably selective aliphatic C-H oxidation reaction for complex molecule synthesis, Science 318 (5851) (2007) 783–787.
[5] Z. Tang, Y. Liu, M. He, W. Bu, Chemodynamic therapy: tumour microenvironment-mediated Fenton and Fenton-like reactions, Angew Chem. Int. Ed. Engl. 58 (4) (2019) 946–956.
[6] H.B. Zeng, S.S. Liu, B.Y. Chai, D. Cao, Y. Wang, X. Zhao, Enhanced photoelectrocatalytic decomplexation of Cu-EDTA and Cu recovery by persulfate activated by UV and cathodic reduction, Environ. Sci. Technol. 50 (12) (2016) 6459–6466.
[7] H.B. Zeng, G. Zhang, Q.H. Ji, H.J. Liu, X. Hua, H.L. Xia, M. Sillanpaa, J.H. Qu, pH-independent production of hydroxyl radical from atomic H$^{\bullet}$-mediated electrocatalytic H_2O_2 reduction: a green Fenton process without byproducts, Environ. Sci. Technol. 54 (22) (2020) 14725–14731.
[8] L. Tian, P. Chen, X.H. Jiang, L.S. Chen, L.L. Tong, H.Y. Yang, J.P. Fan, D.S. Wu, J.P. Zou, S.L. Luo, Mineralization of cyanides via a novel Electro-Fenton system generating $^{\bullet}OH$ and $^{\bullet}O_2^-$, Water Res. 209 (2022) 117890.
[9] G. Zhao, L. Liang, E. Wang, R. Tong, Fenton chemistry for achmatowicz rearrangement, ACS Catal. 11 (6) (2021) 3740–3748.
[10] H. Zeng, Y. Cheng, E. Repo, X. Yu, X. Xing, T. Zhang, X. Zhao, Trace iron as single-electron shuttle for interdependent activation of peroxydisulfate and HSO_3^-/O_2 enables accelerated generation of radicals, Water Res. 223 (2022) 118935.
[11] L. Chen, J. Ma, X. Li, J. Zhang, J. Fang, Y. Guan, P. Xie, Strong enhancement on fenton oxidation by addition of hydroxylamine to accelerate the ferric and ferrous iron cycles, Enviro, Sci. Technol. 45 (9) (2011) 3925–3930.
[12] C. Chen, Y. Wang, Y. Huang, J. Hua, W. Qu, D. Xia, C. He, V.K. Sharma, D. Shu, Overlooked self-catalytic mechanism in phenolic moiety-mediated Fenton-like system: formation of Fe(III) hydroperoxide complex and co-treatment of refractory pollutants, Appl. Catal. B Environ. 321 (2023) 122062.
[13] Y. Gao, P. Wang, Y. Chu, F. Kang, Y. Cheng, E. Repo, M. Feng, X. Yu, H. Zeng, Redox property of coordinated iron ion enables activation of O_2 via in-situ generated H_2O_2 and additionally added H_2O_2 in EDTA-chelated Fenton reaction, Water Res. 248 (2024) 120826.
[14] Z. Guang-Hua, J. Huang-Xian, Y. Bao-Fen, A sensitive fluorescence quenching method for the determination of Iron (II) with 1,10-phenanthroline, Chin. J. Chem. 21 (3) (2010) 301–304.
[15] Y. Lee, R. Kissner, U. von Gunten, Reaction of ferrate(VI) with ABTS and self-decay of ferrate(VI): kinetics and mechanisms, Environ. Sci. Technol. 48 (9) (2014) 5154–5162.
[16] S.X. Peng, M.J. Strojnowski, J.K. Hu, B.J. Smith, T.H. Eichhold, K.R. Wehmeyer, S. Pikul, N.G. Almstead, Gas chromatographic–mass spectrometric analysis of hydroxylamine for monitoring the metabolic hydrolysis of metalloprotease

inhibitors in rat and human liver microsomes, J. Chromatogr. B 724 (1) (1999) 181–187.
[17] F. Weigend, R. Ahlrichs, Balanced basis sets of split valence, triple zeta valence and quadruple zeta valence quality for H to Rn: design and assessment of accuracy, Chem. Chem. Phys. 7 (18) (2005) 3297–3305.
[18] Y. Zhao, D.G. Truhlar, The M06 suite of density functionals for main group thermochemistry, thermochemical kinetics, noncovalent interactions, excited states, and transition elements: two new functionals and systematic testing of four M06-class functionals and 12 other functionals, Theor. Chem. Acc. 120 (1–3) (2007) 215–241.
[19] P. Hirva, M. Haukka, M. Jakonen, M.A. Moreno, DFT tests for group 8 transition metal carbonyl complexes, J. Mol. Model. 14 (3) (2008) 171–181.
[20] A.V. Marenich, C.J. Cramer, D.G. Truhlar, Universal solvation model based on solute electron density and on a continuum model of the solvent defined by the bulk dielectric constant and atomic surface tensions, J. Phys. Chem. B 113 (18) (2009) 6378–6396.
[21] T. Lu, F. Chen, Quantitative analysis of molecular surface based on improved Marching Tetrahedra algorithm, J. Mol. Graph. Model. 38 (2012) 314–323.
[22] T. Brinck, P. Carlqvist, J.H. Stenlid, Local electron attachment energy and its use for predicting nucleophilic reactions and halogen bonding, J. Phys. Chem. A 120 (50) (2016) 10023–10032.
[23] P. Sjoberg, J.S. Murray, T. Brinck, P. Politzer, Average local ionization energies on the molecular surfaces of aromatic systems as guides to chemical reactivity, Can. J. Chem. 68 (8) (1990) 1440–1443.
[24] T. Brinck, J.H. Stenlid, The molecular surface property approach: a guide to chemical interactions in chemistry, medicine, and material science, Adv. Theory Simul. 2 (1) (2018) 1800149.
[25] J. Cao, Q. Ren, F. Chen, T. Lu, Comparative study on the methods for predicting the reactive site of nucleophilic reaction, Sci. China Chem. 58 (12) (2015) 1845–1852.
[26] T. Lu, Q. Chen, Interaction region indicator: a simple real space function clearly revealing both chemical bonds and weak interactions, Chem. Mater. 1 (5) (2021) 231–239.
[27] T. Lu, F. Chen, Multiwfn: a multifunctional wavefunction analyzer, J. Comput. Chem. 33 (5) (2012) 580–592.
[28] W. Humphrey, A. Dalke, K. Schulten, VMD: visual molecular dynamics, J. Mol. Graph. 14 (1) (1996) 33–38.
[29] P.L. Zamora, F.A. Villamena, Theoretical and experimental studies of the spin trapping of inorganic radicals by 5,5-dimethyl-1-pyrroline N-oxide (DMPO). 3. Sulfur dioxide, sulfite, and sulfate radical anions, J. Phys. Chem. A 116 (26) (2012) 7210–7218.
[30] K. Ranguelova, A.B. Rice, A. Khajo, M. Triquigneaux, S. Garantziotis, R.S. Magliozzo, R.P. Mason, Formation of reactive sulfite-derived free radicals by the activation of human neutrophils: an ESR study, Free Radic. Biol. Med. 52 (8) (2012) 1264–1271.
[31] H. Dong, Y. Li, S. Wang, W. Liu, G. Zhou, Y. Xie, X. Guan, Both Fe(IV) and radicals are active oxidants in the Fe(II)/peroxydisulfate process, Environ. Sci. Technol. 7 (3) (2020) 219–224.
[32] H. Zeng, H. Lan, X. An, E. Repo, Y. Park, O. Pastushok, H. Liu, J. Qu, Insight into electroreductive activation process of peroxydisulfate for eliminating organic pollution: essential role of atomic hydrogen, Chem. Eng. J. 426 (2021) 128355.
[33] H. Zhan, R. Zhou, P. Wang, Q. Zhou, Selective hydroxyl generation for efficient pollutant degradation by electronic structure modulation at Fe sites, Proc. Natl. Acad. Sci. 120 (26) (2023) e2305378120.
[34] J.J. Pignatello, E. Oliveros, A. Mackay, Advanced oxidation processes for organic contaminant destruction based on the Fenton reaction and related chemistry, Crit. Rev. Environ. Sci. Technol. 36 (1) (2006) 1–84.
[35] Y. Mang, J.G. Jiang, M.Z. Chen, MINTEQ modeling for evaluating the leaching behavior of heavy metals in MSWI fly ash, J. Environ. Sci. 20 (11) (2008) 1398–1402.
[36] Q. Liu, Y. Li, J. Zhang, Y. Chi, X. Ruan, J. Liu, G. Qian, Effective removal of zinc from aqueous solution by hydrocalumite, Chem. Eng. J. 175 (2011) 33–38.
[37] Z.Y. Li, L. Wang, Y.L. Liu, Q. Zhao, J. Ma, Unraveling the interaction of hydroxylamine and Fe(III) in Fe(II)/Persulfate system: a kinetic and simulating study, Water Res. 168 (2020) 115093.
[38] H. Zeng, X. Zhao, F. Zhao, Y. Park, E. Repo, S.K. Thangaraj, J. Janis, M. Sillanpaa, Oxidation of 2,4-dichlorophenol in saline water by unactivated peroxymonosulfate: mechanism, kinetics and implication for in situ chemical oxidation, Sci. Total Environ. 728 (2020) 138826.
[39] T. Tsuneda, T. Taketsugu, Theoretical investigations on hydrogen peroxide decomposition in aquo, Phys. Chem. Chem. Phys. 20 (38) (2018) 24992–24999.
[40] J. Lati, D. Meyerstein, Oxidation of first-row bivalent transition-metal complexes containing ethylenediaminetetra-acetate and nitrilotriacetate ligands by free radicals: a pulse-radiolysis study, J. Chem. Soc. Dalton Trans. 9 (9) (1978) 1105–1118.
[41] M. Simic, E. Hayon, Intermediated produced from the one-electron oxidation and reduction of hydroxylamines. Acid-base properties of the amino, hydroxyamino, and methoxyamino radicals, J. Am. Chem. Soc. 93 (23) (1971) 159–163.
[42] J. Zou, J. Ma, L. Chen, X. Li, Y. Guan, P. Xie, C. Pan, Rapid acceleration of ferrous iron/peroxymonosulfate oxidation of organic pollutants by promoting Fe(III)/Fe(II) cycle with hydroxylamine, Environ. Sci. Technol. 47 (20) (2013) 11685–11691.
[43] M.C. Diez, D. Pouleurs, R. Navia, G. Vidal, Effect of EDTA and Fe-EDTA complex concentration on TCF Kraft mill effluent degradability. Batch and continuous treatments, Water Res. 39 (14) (2005) 3239–3246.
[44] X. Huang, Y. Xu, C. Shan, X. Li, W. Zhang, B. Pan, Coupled Cu(II)-EDTA degradation and Cu(II) removal from acidic wastewater by ozonation: performance, products and pathways, Chem. Eng. J. 299 (2016) 23–29.
[45] Y. Gao, F. Yang, H. Jian, K. Zhen, P. Zhang, X. Tang, Z. Fu, W. Xu, C. Wang, H. Sun, Pyrene degradation in an aqueous system using ferrous citrate complex activated persulfate over a wide pH range, J. Environ. Chem. Eng. 9 (6) (2021) 106733.
[46] F. Chen, X. Zhao, H. Liu, J. Qu, Reaction of $Cu(CN)_3^{2-}$ with H_2O_2 in water under alkaline conditions: cyanide oxidation, Cu^+/Cu^{2+} catalysis and H_2O_2 decomposition, Appl. Catal. B Environ. 158–159 (2014) 85–90.
[47] F. Chen, X. Zhao, H. Liu, J. Qu, Enhanced destruction of $Cu(CN)_3^{2-}$ by H_2O_2 under alkaline conditions in the presence of EDTA/pyrophosphate, Chem. Eng. J. 253 (2014) 478–485.
[48] M.D. Welman-Purchase, R.N. Hansen, Cyanide within gold mine waste of the free state goldfields: a geochemical modelling approach, Environ. Pollut. 318 (2023) 120825.
[49] X. Liu, X. Xue, Construction and application of a coastline ecological index: a case study of Fujian province, China, Sustainability 16 (2024) 5480.
[50] L. Martínková, P. Bojarová, A. Sedova, V. Křen, Recent trends in the treatment of cyanide-Containing effluents: comparison of different approaches, Crit. Rev. Environ. Sci. Technol. 53 (3) (2022) 416–434.